Contents lists available at ScienceDirect

Applied Catalysis A, General

Towards an efficient selective oxidation of sulfides to sulfones by NiWO$_4$ and α-Ag$_2$WO$_4$

M. Assis [a,b,*], A.F. Gouveia [a], L.K. Ribeiro [a,c], M.A. Ponce [d], M.S. Churio [d], O.N. Oliveira Jr. [b], L. H. Mascaro [c], E. Longo [c], R. Llusar [a], E. Guillamón [a], J. Andrés [a,**]

[a] Department of Analytical and Physical Chemistry, University Jaume I (UJI), Castelló 12071, Spain
[b] São Carlos Institute of Physics, University of São Paulo (USP), 13560-970 São Carlos, SP, Brazil
[c] CDMF-UFSCar, Universidade Federal de São Carlos (UFSCar), P.O. Box 676, CEP, 13565–905, São Carlos, SP, Brazil
[d] Department of Chemistry and Biochemistry, Faculty of Exact and Natural Sciences, Institute of Physics Research of Mar del Plata (IFIMAR) CONICET, Universidad Nacional de Mar del Plata (UNMDP), B7602 Mar del Plata, Argentina

ARTICLE INFO

ABSTRACT

Chemoselective oxidation of sulfides to sulfones under mild conditions is relevant for industry, but challenging owing to the need to establish catalysis mechanisms and optimize several experimental parameters. Herein, we report the synthesis of metal-based tungstates as efficient and selective catalysts for this transformation in darkness. This catalytic process is tolerant of a broad range of functionalized substituted sulfides even in the presence of oxidative-sensitive functional groups. α-Ag$_2$WO$_4$ and NiWO$_4$ were found to be the best performing catalysts due to good selectivity, stability, and yield under very mild conditions, completing the transformation in 1 and 2 h, respectively. The key success of the selective oxidation is attributed to hydroxyl radical and singlet oxygen (•OH and ^{1}O$_2$), as the redox mediators along a two-step process. These findings open a pathway for oxidation processes on semiconductors in complete darkness, overcoming the limitation of light, being required in a wide range of applications.

1. Introduction

Designing and developing efficient and robust, and at the same time, easily synthesized, low-cost, nontoxic, and highly effective catalysts for the selective oxidation of sulfides to sulfones is urgently needed when thinking about the emergence of viable technologies. Sulfoxides and sulfones play a key role in modern organic chemistry, fine chemicals, pharmaceutical, agrochemical industry and functional materials [1–7]. Indeed, numerous protocols for the synthesis of sulfoxides and sulfones, where a wide variety of catalysts, such transition-metal salts [8,9], metal complexes [4,10], noble metal complexes, metal-organic frameworks (MOFs) [11,12], covalent organic frameworks (COFs) [13], poly-oxometalates [14,15], mesoporous silica MCM-41 [16], C$_3$N$_4$ nano-sheets [17], VO$_x$/SiO$_2$ and VO$_x$/Al$_2$O$_3$ [18] can be found in the literature.

The most traditional approach to synthesize these organosulfur compounds are based on the chemoselective oxidation of sulfides. However, these processes require the use of oxidants, such as halogen derivatives and peracid or inorganic oxidative reagents [19], which are not eco-friendly or cause serious environmental pollution. Also, these oxidants impact in the environment, economy, reaction controllability, and selectivity, [15,20,21] generate dangerous waste. At this point, it is necessary to highlight the importance of developing greener and sustainable methods [22].

Metal oxides as semiconductors are actively being studied as photocatalysts [23–25]. Among them, metal tungstates attract the attention of researchers due to their ability to operate in both ultraviolet and visible light [26–28]. Recently, Kang et al. [29] have decorated WO$_3$ with transition metal tungstate MWO$_4$ (M = Cu, Zn, Ni), and they found that MWO$_4$/WO$_3$ photocatalysts showed a higher activity for photocatalytic oxidative desulfurization of dibenzothiophene than pure WO$_3$ or MWO$_4$ under visible light irradiation. Very recently, Lima et al. [30] have reported that the thioanisole was oxidized by hydrogen peroxide to sulfoxides and sulfones and the presence of MWO$_4$ (M = Cu, Zn, Ni) as catalyst accelerates the conversion.

Our group is engaged in a research project to investigate the

---

* Corresponding author at: Department of Analytical and Physical Chemistry, University Jaume I (UJI), Castelló 12071, Spain.
** Corresponding author.
E-mail addresses: marcelostassis@gmail.com (M. Assis), andres@qfa.uji.es (J. Andrés).

structure, properties, and different applications of a family of metal tungstates [31–34] of general formula MWO$_4$ (M = Cu, Cd, Co, Mn, Ni, and Zn) or M$_2$WO$_4$ (M = Ag). These compounds combine two metal cations with oxygen anions and charge balanced stoichiometry with complex structures and promising properties for a broad range of applications. MWO$_4$ (M = Cd, Co, Mn, Ni, and Zn) oxides have a monoclinic wolframite structure with primitive cell composed by an arrangement of [MO$_6$] and [WO$_6$] octahedral clusters [33,34], while CuWO$_4$ presents a triclinic structure [35]. On the other hand, Ag$_2$WO$_4$, in its most thermodynamic phase (α-Ag$_2$WO$_4$), presents an orthorhombic structure, with high complexity due to the large number of different atomic arrangements in its lattice, such as [AgO$_x$] (x = 2, 4, 6, and 7) and [WO$_6$] clusters [36–38]. These structural features confer unique properties to each tungstate salt, which are highly utilized for various applications, such as solar cells [39], battery materials [40], supercapacitors [40,41], photocatalysts [32,42], water splitting [43], and electrochemical sensors [44], due to its advantages, such as limitless resources, tailorable surface, low cost, low toxicity, good chemical stability, large specific capacitance, and environmental friendliness.

Based on these structural characteristics, we envisioned that metal tungstates would be appropriate candidates to speed up advanced oxidation processes in the heterogeneous medium, even in the darkness. It is expected that they have better catalytic performance than simple metal oxides due to their complex chemical composition and synergy between metals. Once succeeded, such a scenario not only provides an effective and concise protocol for the selective oxidation of sulfides to sulfones, but also offers an unrecognized opportunity in catalytic functionalization of sulfones resulting from the kinetics of the intrinsic substrate reactivity. To check the validity of our hypothesis, in this work, we present the investigation of wolframite structures (MWO$_4$, M = Cd, Co, Cu, Mn, Ni, and Zn) and α-Ag$_2$WO$_4$, as catalysts for the selective oxidation of sulfides to sulfoxides or sulfones in the dark. We believed that the present approach not only represents a clean and economical method for the synthesis of sulfones, but also exhibited promising prospects in synthetic chemistry. In addition, catalytic stability, scaling and leaching tests have been performed. Finally, results from scavenger experiments, radical probes and paramagnetic resonance spectroscopy have allowed us to propose the most plausible mechanism for this transformation. This investigation can unravel the origin of the oxidation process for developing new metal oxides as catalysts.

2. Experimental section

2.1. Materials

MWO$_4$ (M = Cd, Co, Cu, Mn, Ni, and Zn) and α-Ag$_2$WO$_4$ catalysts were synthesized through the coprecipitation (CP) method in an aqueous medium followed by microwave irradiation (MI) according to literature methods [45]. All metal-based precursors, scavengers and reagents were purchased at Sigma-Aldrich except the AgNO$_3$ which was obtained from Cenabras and were used without further purification.

2.2. Catalyst characterization

The powder X-ray diffraction (XRD) patterns of the catalysts were acquired with a Rigaku diffractometer, Japan, model DMax2500PC. Raman spectroscopy provided structural information using the Horiba Jobin-Yvon spectrometer, Japan, model T64000, coupled with the CCD Synapse and argon-ion laser detector, operating at 514 nm. The morphology and texture of the catalyst were observed by field emission scanning electronic microscopy (FE-SEM) operated at 10 kV (Supra 35-VP, Carl Zeiss). Diffuse reflectance spectroscopy (DRS) was performed using a Cary 5 G spectrophotometer. Transmission electronic microscopy (TEM) images were obtained by using a Jeol JEM-2100 F operating at 200 kV. The superficial area was recorded with a TRISTAR 3000 (Micromeritics) at a temperature of 150 °C by N$_2$ adsorption/desorption

isotherms using Brunauer–Emmett–Teller (BET) methodology.

2.3. Catalytic oxidation of sulfides

At the start of our catalytic studies, the oxidation of methyl phenyl sulfide or thioanisole (**1a**) with hydrogen peroxide was used as a benchmark system for the optimization of the conditions using different catalysts. The effect of the temperature (30, 50 and 70 °C), time (0.5, 1 and 2 h), H$_2$O$_2$ concentration and catalyst loading were evaluated (see also the Supporting Information). Methyl phenyl sulfide (0.1 mmol) was dissolved in the specified solvent (2 mL); next, the selected catalyst (10 or 15 mg) and various amounts (1.2 and 2.4 mmol) of H$_2$O$_2$ volume (30% v/v) were added to the reaction mixture. Reactions were performed it in a 4 mL round-bottom flask with a septum and constant magnetic stirring of 700 rpm/min and constant temperature. At the end of the reaction, an aliquot of 0.5 mL was taken, centrifuged at 6000 rpm for 2 min, filtered and redispersed in 1 mL of ethyl acetate. The progress of the oxidation reaction was monitored by gas chromatography (GC, Agilent 8860) provided with a flame-ionization detector (FID), using a non-polar (5%-phenyl)-methylpolysiloxane column (Agilent J&W HP-5). The methods used in the GC for the detection of the products can be found in the Supporting Information. To evaluate the catalytic substrate scope, commercial sulfides and sulfones were used for GC calibration. The scavenger experiments were carried out following the same procedure in the presence of equimolar amounts of scavengers.

For the catalyst recycling experiment, the reaction was scaled ten times for a best recovery of the catalyst after each cycle. Reaction were performed in a 30 mL round-bottom flask with a septum under constant stirring at 700 rpm at 50 °C for 1 h. When the used catalyst was α-Ag$_2$WO$_4$, 1 mmol of thioanisole, 100 mg of catalyst, 1 mL of H$_2$O$_2$ (30% v/v), 150 µL of hexadecane and 20 mL of acetonitrile were used. When the catalyst used was NiWO$_4$, the catalyst loading was changed to 150 mg and the reaction time to 2 h. After the end of the catalytic cycle, an aliquot was taken and analyzed by GC. For recovery of the catalyst after the end of each cycle, the suspension was centrifuged at 6000 rpm for 2 min, removing the supernatant and washing 3 times with acetonitrile through redispersion followed by centrifugation. The catalyst was then dried at 60 °C for 12 h and reused again for 10 catalytic cycles without adding any other components.

2.4. ICP-OES analysis

The chemical composition of the solutions after the 1st, 5th, and 10th catalytic cycles was estimated by inductively coupled plasma optical emission spectrometry (ICP OES) using an ICP OES iCAP 7000 (Thermo Fisher Scientific, USA).
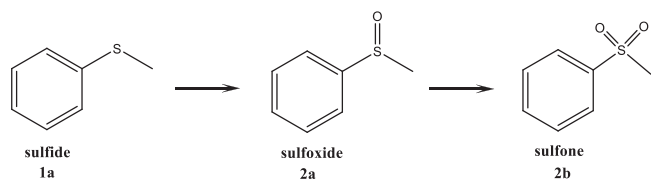
2.5. Singlet oxygen detection

Detection of singlet oxygen (^{1}O$_2$) was performed in the dark by adding the catalyst to a solution containing 9,10-dimethylanthracene (2 mL, 3×10^{-3} M in acetonitrile) and H$_2$O$_2$ (100 µL) and using the optimized conditions. Different aliquots were removed at 10, 20, 30, and 60 min and analyzed by absorption spectrophotometry in the UV-Visible region.

2.6. Hydroxyl radical detection

For detection of hydroxyl detection (•OH), 10 µL of a solution of 5,5-dimethyl-1-pyrroline N-oxide (DMPO) was placed in contact with the oxidant and also with a mixture of oxidant and catalyst. The experiment was carried out in the dark under the optimized conditions. An aliquot of this mixture placed in a cylindrical quartz tube was examined by Electron Paramagnetic Resonance (EPR) with the following settings: 9.59816 GHz frequency; 100 kHz modulation frequency; 3420 G central field; 200 G sweep width; 2 G modulation amplitude; 40 ms conversion

Table 1
Morphology and size of different catalysts.

Catalyst	Morphology	Size (nm)
α-Ag$_2$WO$_4$	Rods	422.8 × 135.4
CdWO$_4$	Rods	183.3 × 82.4
CoWO$_4$	Irregular polyhedral	33.6
CuWO$_4$	Irregular polyhedral	168.5
MnWO$_4$	Rods	56.2 × 27.3
NiWO$_4$	Irregular polyhedral	19.7
ZnWO$_4$	Irregular polyhedral	21.6

Scheme 1. – Thioanisole oxidation reaction.

time; 41 s sweep time; 10 dB attenuation and 20.37 mW power. The spectrum was obtained after averaging 20 scans.

3. Results and discussion

3.1. Catalyst characterization and performance

All catalysts were synthesized following the reported procedures and were characterized by the usual techniques, namely, XRD and FE-SEM (see Figs. S1-S7, Supporting Information). The most relevant data from the FE-SEM are summarized in Table 1. All materials have nanometric averaged size, except α-Ag$_2$WO$_4$ and CuWO$_4$, and an irregular morphology, except α-Ag$_2$WO$_4$, CdWO$_4$ and MnWO$_4$, which present a rod morphology.

The catalytic activity of the tungstates was evaluated for the methyl phenyl sulfide (thioanisole) oxidation as a model reaction. Thioanisole oxidation to the corresponding sulfone consists in a two-step process, which involves a sulfoxide intermediate (2a, Scheme 1). The first step is a relatively very facile process and, in general, occurs at low temperatures in the presence of a stoichiometric amount of oxidant. However, complete oxidation to sulfone (2b, Scheme 1) requires more severe
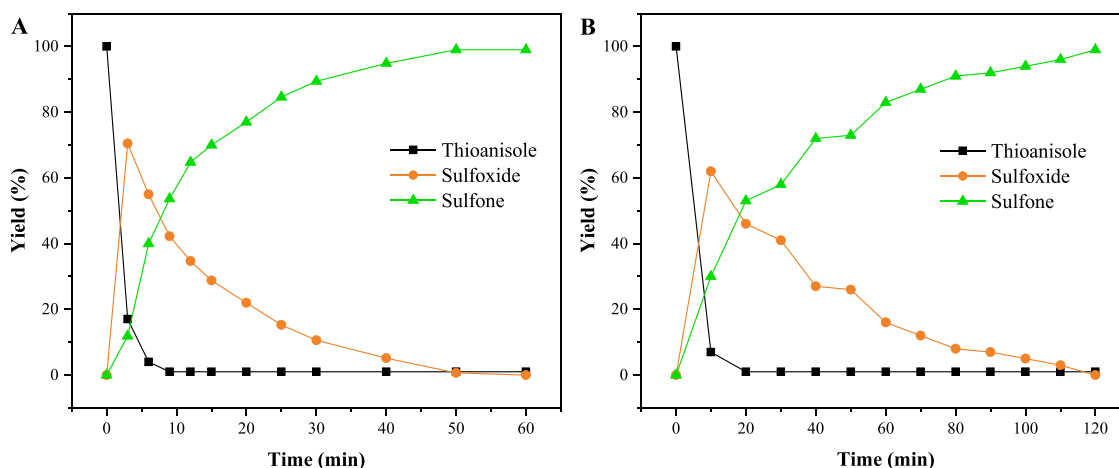
Table 2
Time and temperature dependence for thioanisole oxidation.[a]

Entry	Catalyst	Time (h)	Temperature (°C)	Conversion (%)[b]	Yield (%)[b]	
					2a	2b
1	CoWO$_4$	2	30	58	52	6
2	α-Ag$_2$WO$_4$ CuWO$_4$	1	50	89	75	14
3				74	64	9
4	CdWO$_4$	2	50	88	58	29
5	MnWO$_4$			83	57	26
6	NiWO$_4$			92	56	36
7	ZnWO$_4$			60	46	14

[a] Reaction conditions: 1a (0.1 mmol), H2O2 (1.2 mmol), CH3CN (2 mL), 10 mg of catalyst.
[b] Determined by GC-FID analysis using hexadecane as an internal standard.

Table 3
Optimizing oxidizing concentration, solvent, and catalyst mass for sulfide oxidation.[a]

Entry	Catalyst	[H$_2$O$_2$] (mmol)	Catalyst loading	Solvent	Conversion (%)[b]	Yield (%)[b]	
						2a	2b
1[i]	α-Ag$_2$WO$_4$	2.4	10	CH$_3$CN	> 99	0	99
2[iii]	CdWO$_4$	2.4	15	CH$_3$CN	> 99	13	85
3[ii]	CoWO$_4$				91	64	27
4[i]	CuWO$_4$				97	50	48
5[iii]	MnWO$_4$				> 99	33	67
6[iii]	NiWO$_4$				> 99	0	99
7[iii]	ZnWO$_4$				> 99	31	68

[a] Reaction conditions: 1a (0.1 mmol), H2O2 (2.4 mmol), solvent (2 mL).
[b] Determined by GC-FID analysis using hexadecane as an internal standard. i Reaction time = 1 h and T = 50 °C; ii Reaction time = 2 h and T = 30 °C; iii Reaction time = 2 h and T = 50 °C.

Fig. 1. Kinetics of thioanisole oxidation by H_2O_2 catalyzed by: A) α-Ag_2WO_4; B) $NiWO_4$.

reaction conditions [46]. Besides this, most common oxidants employed to carry out this transformation, such peracids or meta-chloroperbenzoic acid (m-CPBA) are considered not sustainable. In this work we used H_2O_2 as oxidant, which is considered much more eco-friendly.

Optimization of the reaction conditions was carried out by varying the oxidant and catalyst amounts, temperature, solvent, and time (Table S1 and S2, Supporting Information) starting from 0.1 mmol of thioanisole, 1.2 mmol of H_2O_2, 10 mg of catalyst and 2 mL of CH_3CN. Temperature was an important parameter to get the best conversion values and although in most cases at 70ºC conversion reaches the best results, differences are only slight with those obtained at 50ºC. So, considering the economic impact that causes an increase of 20ºC, 50ºC was adopted as the optimum temperature. Further, catalytic conversion was time dependent for all catalysts being the more efficient at 50ºC the α-Ag_2WO_4 and $CuWO_4$ powders, with values of 89% and 74%, respectively, after 1 h of reaction (entries 15,18, Table S1, Supporting Information). Increasing temperature or reaction time doesn't cause any effect on the selectivity being the main product the methyl phenyl sulfoxide intermediate (entries 22–42 Table S1, Supporting Information). The main results can be seen in Table 2.

Oxidizing reagent concentration, solvent and catalyst loading were also optimized (Table S2, Supporting Information). The main results are listed in Table 3. Changing acetonitrile by methanol, THF or dichloromethane reduces considerably the catalyst activity (entries 1–21, Table S2 Supporting information). Considerable increase in the

selectivity was achieved by duplicating the amount of oxidizing reagent (entries 1 and 6, Table 3 and Table S2, Supporting Information). Control experiments confirmed that both, oxidant and catalyst are required to carry out the oxidation reaction (entries 29–31, 39–41 and 49–51 and 52–58, Table S2, Supporting Information). Although all the materials improve their selectivity towards the sulfone under these new conditions, the most effective catalyst was the α-Ag_2WO_4 completing the transformation in 1 h in CH_3CN, in the presence of 2.4 mmol H_2O_2 (entry 1, Table 3). Also, quantitative yield of the sulfone product was obtained in the presence of $NiWO_4$ after 2 h and using 15 mg of the catalyst (entry 6, Table 3).

3.2. Kinetics, Recyclability and Scope

The kinetics of thioanisole oxidation mediated by α-Ag_2WO_4 and $NiWO_4$ under optimal conditions is shown in Fig. 1. It is noteworthy that 83% of thioanisole reacts within 3 min in the presence α-Ag_2WO_4, 12% of which corresponds to methyl phenyl sulfone. Total conversion of methyl phenyl sulfoxide into methyl phenyl sulfone occurs in 50 min, which represents a high oxidation efficiency in a short period of time at relatively low temperature. A similar profile is obtained for $NiWO_4$, but longer reaction time is needed. These data suggests that the limiting step for the reaction is the oxidation of methyl phenyl sulfoxide intermediate to methyl phenyl sulfone, as reported by Liang et al. [1]. Table S3 shows the comparison with other previously published works that use
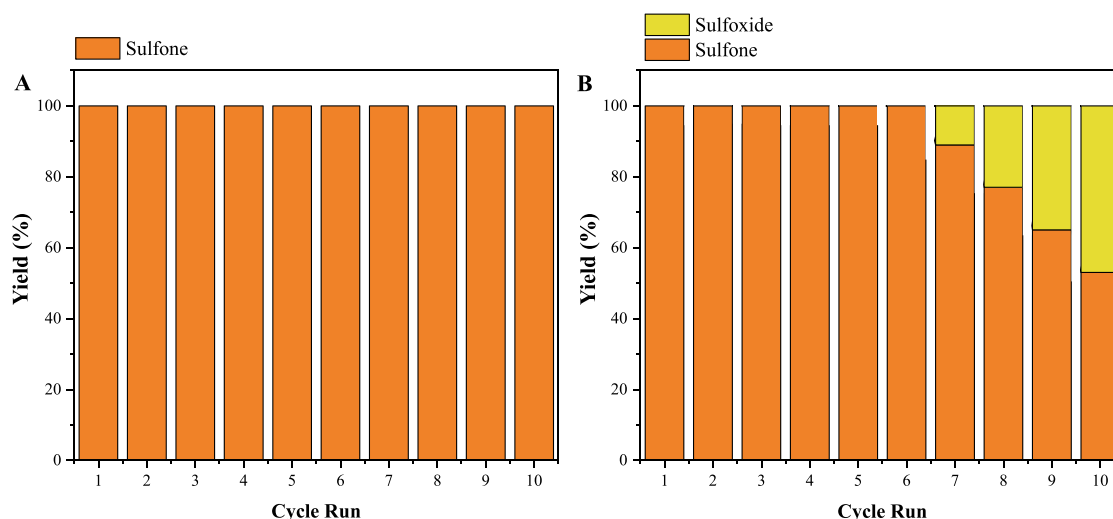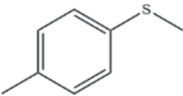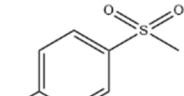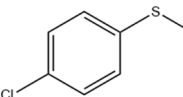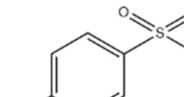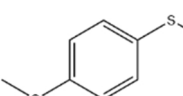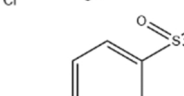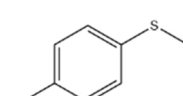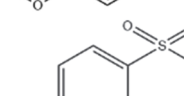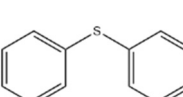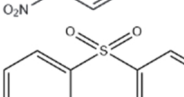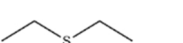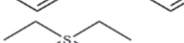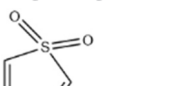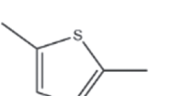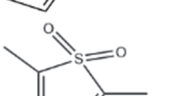

Fig. 2. Recycling of catalyst in thioanisole oxidation: A) α-Ag_2WO_4 and B) $NiWO_4$.

Table 4

Catalytic scope for the sulfide oxidation reaction mediated by α-Ag₂WO₄ and NiWO₄.[a]

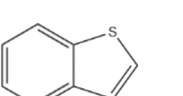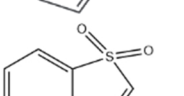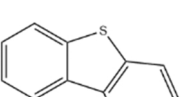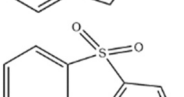| Entry	Substrate	Product	α-Ag₂WO₄[i] Time (h)	C (%)[b]	Y (%)[b]	NiWO₄[ii] Time (h)	C (%)[b]	Y (%)[b]
1			1	98%	98%	2	99%	99%
2			1	> 99%	99%	2	96%	96%
3			1	97%	97%	2.5	98%	97%
4			1	> 99%	98%	2	> 99%	99%
5			2	> 99%	99%	4	97%	96%
6			2	> 99%	99%	3	> 99%	99%
7			2	92%	89%	4	94%	80%
8			2	94%	91%	5	95%	86%
9			3	91%	90%	6	92%	77%
10			3	92%	87%	6	88%	75%

[a] Reaction conditions: Substrate (0.1 mmol), H2O2 (2.4 mmol), CH3CN as solvent (2 mL) and 50ºC.

[b] Determined by GC-FID analysis using hexadecane as an internal standard. i Reaction time = 1 h and 10 mg; ii Reaction time = 2 h and 15 mg.

semiconductors or semiconductor-based heterostructures for the oxidation of thioanisole.

As shown in Fig. 2A, the α-Ag₂WO₄ catalyst can be recycled up to 10 successive runs without lost in the efficiency, revealing high stability and robustness during the catalytic cycles. The total turnover number (TON) [39] for α-Ag₂WO₄ was 4.63 cycles, showing high performance of the catalyst on reuse under continuous operation. Since the reaction is performed within 60 min, the turnover frequency (TOF) is 0.077 min^{-1} [47]. The efficiency of NiWO₄ (Fig. 2B) remains invariable up to 6 runs after which the catalyst losses selectivity. In this case, TON was 2.05 cycles, until the 6th cycle, and TOF was 0.017 min^{-1}.

Inductively coupled plasma optical emission spectroscopy (ICP-OES) was used to analyze the possibility of metal leaching (Table S4, Supporting Information). These analyses, carried out after centrifugation of a sample after the 1st, 5th, and 10th run cycles, revealed that the concentrations of Ag and W atoms in α-Ag₂WO₄ are practically constant during catalytic recycling, with much larger number of W atoms than Ag

atoms. The number of W atoms corresponds to approximately 1.6% of the initial mass of the catalyst, i.e., 1.6% leaching of the catalyst occurs per catalytic cycle. Similar results were obtained for NiWO₄, but both metals were leached at the same proportion, with a leaching of approximately 1.8% of the initial mass of the catalyst per cycle. This data suggests that oxidation is not caused by the ionic species in solution, as indicated by adding equimolar amounts of Ag$^+$, Ni^{2+} and (WO₄)$^{2-}$ to the catalyst and observing conversions similar to that of H₂O₂ without catalyst (see Table S5, Supporting Information).

Heterogeneous catalysts for the oxidation of sulfides present advantages over the homogeneous counterpart as they interact with the oxidazing reagent without suffering any transformation. This prompted us to extend the substrate scope to aromatic and aliphatic R^1—S—R^2 (R^1, R^2 = alkyl, aryl) sulfides. Substituted thioanisole derivatives in Table 4 (entries 1–4) were oxidized quantitatively to the corresponding sulfone products under the optimized reaction conditions independently of the substituent on the aromatic ring requiring twice the time by replacing
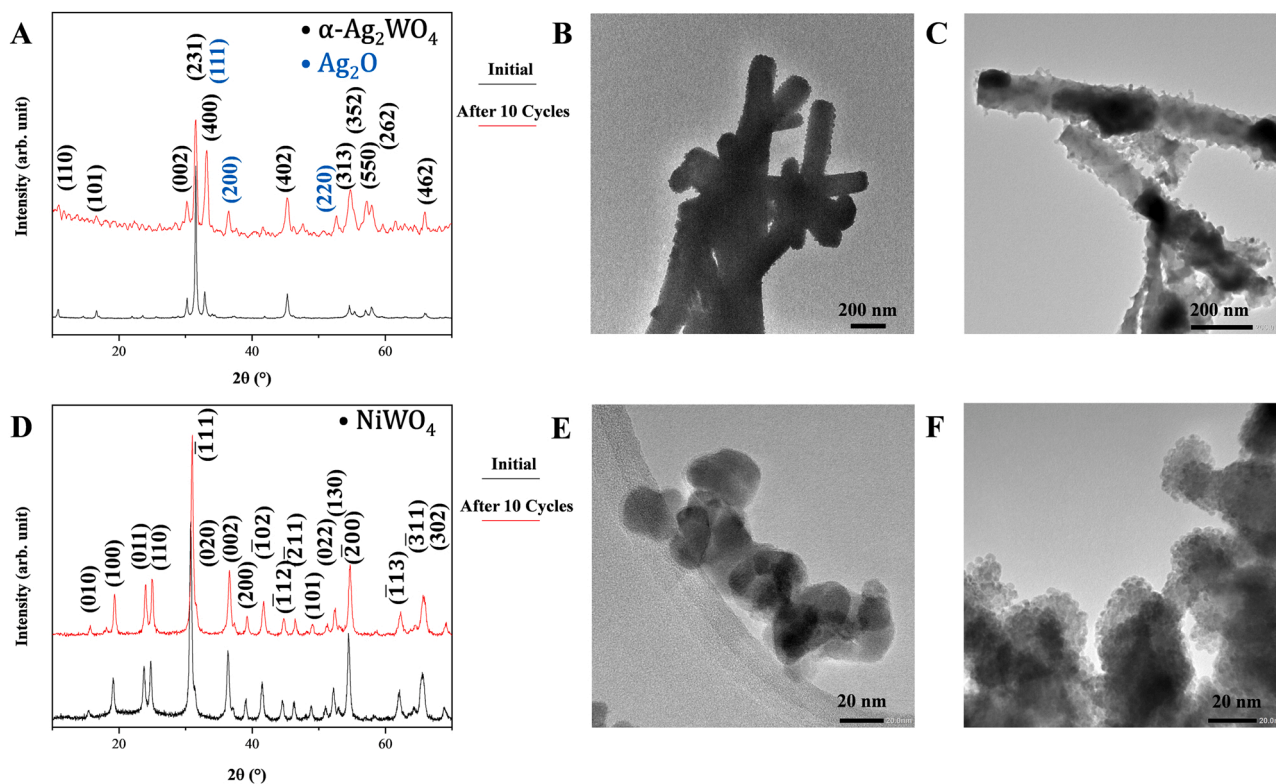
Fig. 3. XRD am TEM images of the catalyst before and after catalytic recycling; A-C) α-Ag$_2$WO$_4$ and D-F) NiWO$_4$.

α-Ag$_2$WO$_4$ by NiWO$_4$ catalyst. However, symmetric aromatic, aliphatic thioethers and cyclic sulfides based on thiophene (entries 5–10, Table 4) need longer reaction time to afford quantitative sulfone yields for both catalysts. It is remarkable that other heterogeneous catalysts need further additives, such a co-oxidant, or longer reaction times or higher temperatures to afford this oxidation reaction.

As aforementioned, no metal leaching has been proved by ICP-OES analyses. However, the oxidation process affected the morphology and structure of the catalysts. The formation of cubic Ag$_2$O according to the XRD in Fig. 3A indicates that α-Ag$_2$WO$_4$ undergoes modifications during the oxidative process. Furthermore, the TEM images in Fig. 3B-C show that the initial morphology of hexagonal rods is deteriorated due to
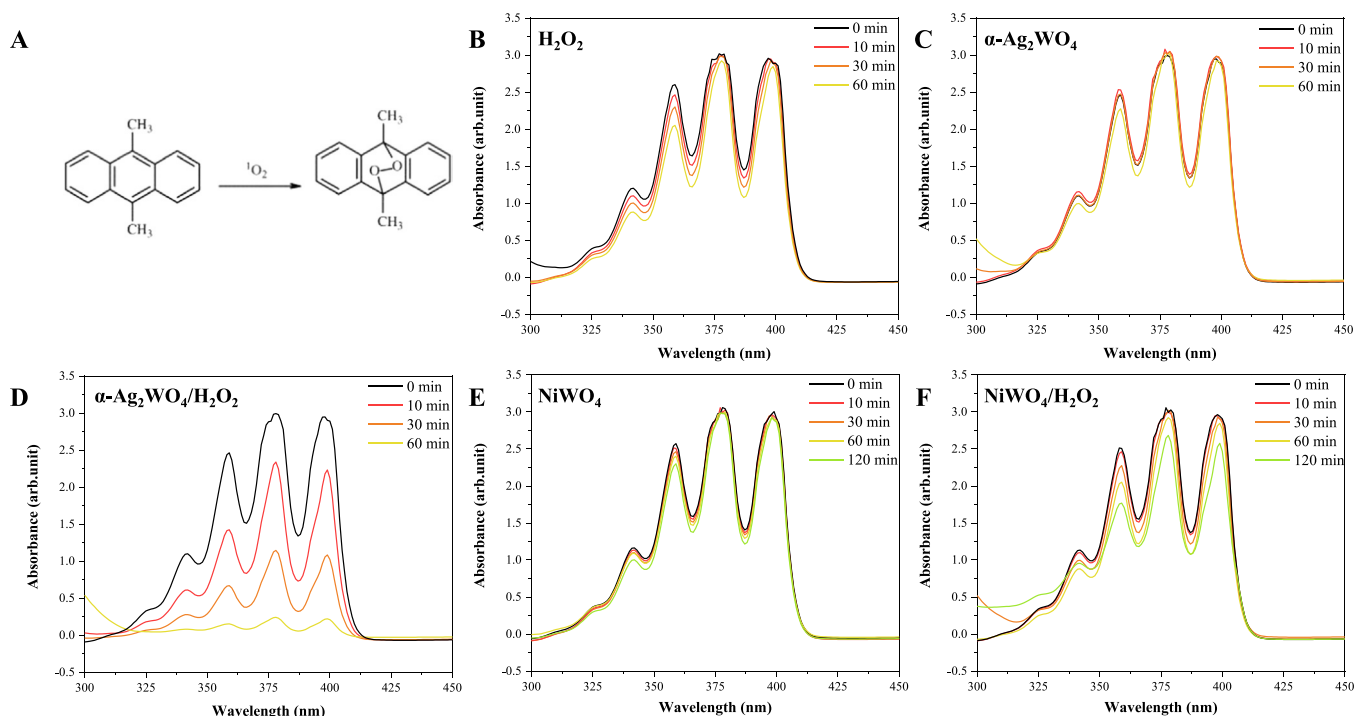

Fig. 4. UV-Vis spectra using DMA as ^{1}O$_2$ indicator as the reaction shown in A) for B) H$_2$O$_2$, C) α-Ag$_2$WO$_4$, D) α-Ag$_2$WO$_4$/H$_2$O$_2$, E) NiWO$_4$, and F) NiWO$_4$/H$_2$O$_2$.
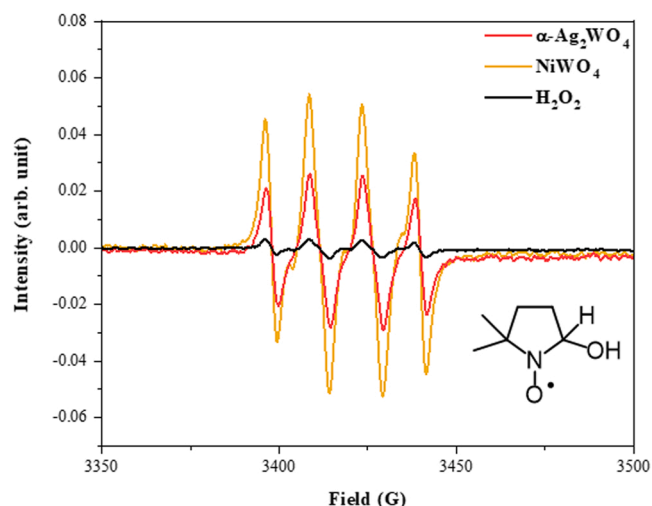
Fig. 5. Detection of •OH using DMPO by EPR.

oxidation. The α-Ag$_2$WO$_4$/Ag$_2$O interface formed during oxidation remains effective for the oxidation of sulfides. This is consistent with ICP-OES results with a small part of α-Ag$_2$WO$_4$ decomposing into interfacial Ag$_2$O, and (WO$_4$)$^{2-}$ in solution. The XRD data in Fig. 3D for NiWO$_4$ do not support formation of other phases or changes in structure. However, the TEM images in Fig. 3E-F show degradation of the initial morphology and agglomeration of the samples. Thus, morphology degradation impairs the oxidation reaction stability of NiWO$_4$.

3.3. Proposed mechanism

Electronic excitation of a semiconductor occurs through formation of electron−hole (e$^-$–h$^+$) pairs, which can interact with the molecules surrounding its chemical environment [35,48]. For α-Ag$_2$WO$_4$ and NiWO$_4$, the band gap energy (E$_{gap}$) needs to be overcome to form e$^-$–h$^+$ pairs. These can be generated through external sources of excitation such as light, temperature and pressure [49]. In this work, the e$^-$–h$^+$ pairs available to trigger highly reactive cascade reactions are obtained through thermoexcitation. To help understand the free radical production mediated by α-Ag$_2$WO$_4$ and NiWO$_4$, and obtain mechanistic clues about the oxidation of thioanisole, the presence of ^{1}O$_2$ and •OH radicals was monitored. The presence of ^{1}O$_2$ was determined by using 9,

10-dimethylanthracene (DMA), which reacts specifically with ^{1}O$_2$ to form a stable endoperoxide [50]. The decrease in absorbance of DMA (between 300 and 420 nm) is used as a measure of endoperoxide formation [51]. Fig. 4 shows no decrease in DMA absorption for the separate oxidizer (H$_2$O$_2$) and semiconductor (α-Ag$_2$WO$_4$ and NiWO$_4$). However, there is a sudden decrease in DMA absorption for the mixture of α-Ag$_2$WO$_4$ and H$_2$O$_2$, indicating a synergistic effect for the generation of ^{1}O$_2$ within the reaction time (60 min). For NiWO$_4$, there is a slight reduction in the intensity of the maximum reaction time (120 min) related to the initial one, showing that the efficiency of NiWO$_4$, when combined with H$_2$O$_2$, is lower for the generation of ^{1}O$_2$.

In situ EPR is suitable to determine •OH radical species during the catalytic processes. The EPR spectra in Fig. 5 indicate that the •OH radical was captured by DMPO, and •OH signals are not found without addition of the catalysts. Signals assigned to DMPO-OH adduct are only seen when α-Ag$_2$WO$_4$/NiWO$_4$ and H$_2$O$_2$ are combined [52]. Since the EPR spectra are presented as first derivatives of the absorption resonance modes, their double integration must be performed to obtain the area under the absorption curve as a measure of the total intensity. The double integration of the signals between 3380 G and 3460 G provides the values (expressed in arbitrary units) referring to the production of •OH radicals for NiWO$_4$ (50.18) and for α-Ag$_2$WO$_4$ (27.92). In contrast to the generation of ^{1}O$_2$, NiWO$_4$ can generate practically twice as many •OH radicals compared to α-Ag$_2$WO$_4$, using the amount of catalyst optimized for the reaction. It is worth noting that both ^{1}O$_2$ and •OH interact differently with the sulfide. From the results shown in Figs. 4 and 5 it is assumed that ^{1}O$_2$ is more efficient to oxidize sulfides than •OH, since α-Ag$_2$WO$_4$ exhibits higher catalytic activity with less catalyst mass and shorter reaction time. Both •OH and ^{1}O$_2$ are powerful oxidants capable of oxidizing a wide range of organic compounds, but ^{1}O$_2$ is much more selective than •OH [53]. It is important to note that the catalytic activity in the sulfide oxidation reaction using these catalysts is not dependent only on the surface area of the catalyst, since α-Ag$_2$WO$_4$ (0.4 m^2/g) has a much smaller surface area than NiWO$_4$ (128 m^2/g), but also the electronic structure of these semiconductors.

To verify whether the detected ^{1}O$_2$ and •OH radicals participate directly or indirectly in thioanisole oxidation, specific scavenger experiments were performed for e$^-$ [54], h$^+$ [35,48], ^{1}O$_2$ [55], and •OH [56] in equimolar amounts to the substrate (Table 5). Tests with higher concentrations of scavengers were performed, but minimal differences were observed. It is not possible to measure the number of surface-active sites in the semiconductor for the generation of these species; then, any reduction in conversion/yield indicates participation of the specific

Table 5
Influence of the scavenger on the catalytic oxidation of thioanisole.[a]

Entry	Catalyst	Scavenger	Scavenged Species	Conversion (%)[b]	Yield (%)[b] 2a	2b
1	α-Ag$_2$WO$_4$[i]	–	–	> 99	0	99
2		AgNO$_3$	e$^-$	54	38	15
3		NaN$_3$	^{1}O$_2$	37	20	16
4		(NH$_4$)$_2$C$_2$O$_4$	h$^+$	52	35	15
5		PHP	• OH	44	30	13
6		PHP + NaN$_3$	• OH +^{1}O$_2$	7	5	0
7	NiWO$_4$[ii]	–	–	> 99	0	99
8		AgNO$_3$	e$^-$	34	26	7
9		NaN$_3$	^{1}O$_2$	96	9	86
10		(NH$_4$)$_2$C$_2$O$_4$	h$^+$	26	19	7
11		PHP	• OH	29	21	5
12		PHP + NaN$_3$	• OH +^{1}O$_2$	10	9	0

[a] Reaction conditions: 1a (0.1 mmol), H2O2 (2.4 mmol), CH3CN (2 mL) and 50ºC.
[b] Determined by GC-FID analysis using hexadecane as an internal standard. i Reaction time = 1 h and 10 mg; ii Reaction time = 2 h and 15 mg.
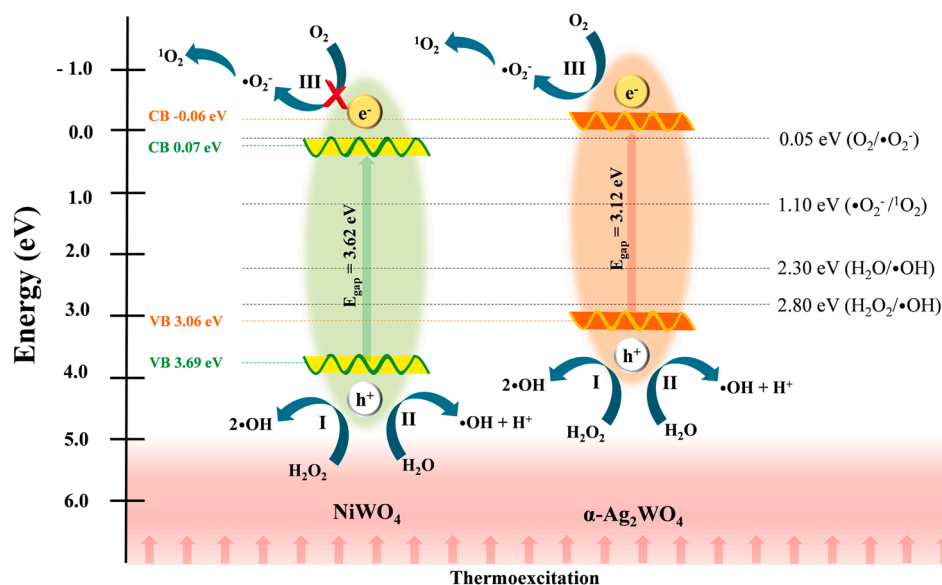
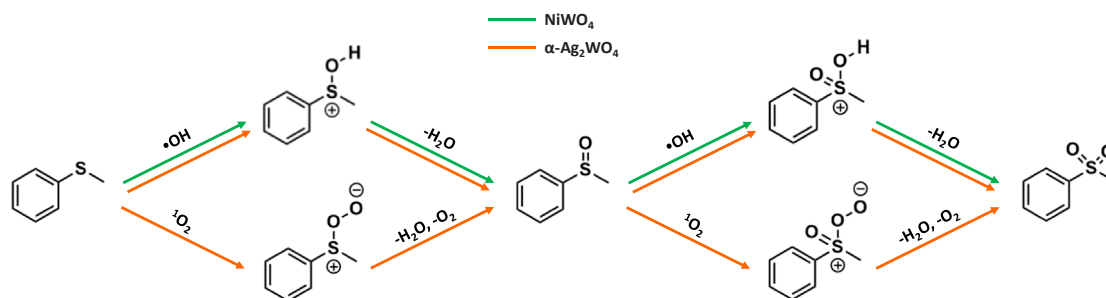**Fig. 6.** Positions of the CB and VB of the catalysts compared with the redox potentials of ROS formation.

Fig. 7. Mechanism of thioanisole oxidation from $^1O_2$ and •OH radical.

species in the oxidation process. The mechanism of thermoexcitation and generation of e^-–h^+ pairs is supported by the result of scavenger (AgNO$_3$ and (NH$_4$)$_2$C$_2$O$_4$, for e^- and h^+, respectively) owing to the significant reduction in conversion and formation of methyl phenyl sulfone. The radical $^1O_2$ plays a significant role in thioanisole oxidation for α-Ag$_2$WO$_4$ due to the decreased catalytic efficiency using NaN$_3$ as $^1O_2$ scavenger [55]. These results corroborate the observations made from Fig. 4. For the scavenger potassium hydrogen phthalate (PHP), which is selective for •OH radical, there was also a reduction in catalytic efficiency for both catalysts [56]. When PHP was mixed with NaN$_3$, a sharp reduction in catalytic efficiency was observed, confirming that the main oxidation pathway is caused by •OH radical and $^1O_2$.

When H$_2$O$_2$ is added as an oxidizer, its decomposition gives rise to O$_2$ and H$_2$O [57]. These species can interact with the e^-–h^+ pairs generated in the conduction (CB) and valence (VB) bands of the semiconductor, giving rise to reactive oxygen species (ROS). The possibility of NiWO$_4$ and α-Ag$_2$WO$_4$ to generate these radicals was verified by performing DRS measurements whose results were analyzed with the Kubelka-Munk method to determine E$_{gap}$ [58]. The E$_{gap}$ values were 3.62 and 3.12 eV for NiWO$_4$ and α-Ag$_2$WO$_4$ respectively, from which the energy of CB and VB was calculated using Mulliken's electronegativity theory to compare with the redox potentials of ROS formation [59]. Fig. 6 shows that both semiconductors have E$_{gap}$ compatible with the oxidation of H$_2$O$_2$ and H$_2$O to form •OH radicals (reactions I and II in Fig. 6). Only α-Ag$_2$WO$_4$ is capable of forming $^1O_2$, since the process depends on the reduction of O$_2$ in CB to form a superoxide radical (•O$_2^-$), which is then oxidized to form the $^1O_2$ (reaction III in Fig. 6). These results are in line with the EPR analysis, scavengers and •OH radical

probe, and help to explain the catalytic differences between NiWO$_4$ and α-Ag$_2$WO$_4$.

Conclusions extracted from all the scavengers and probes experiments have allowed us to propose a plausible mechanism for the oxidation of sulfides, as the one illustrated in Fig. 7. Sulfones can be obtained in two ways through two consecutive oxidation steps. The first way consists in the addition of the •OH radical to the sulfide (and then to the sulfoxide) followed by subsequent elimination of H$_2$O due to the capture of H$^+$ by another •OH radical. The second pathway starts from $^1O_2$, from its addition to sulfur, followed by subsequent elimination of H$_2$O and O$_2$ due to interaction of the eliminated O atom with H$_2$O$_2$ of the reaction medium. While the first pathway occurs for both NiWO$_4$ and α-Ag$_2$WO$_4$ catalysts, since both are •OH generators the second, which is more effective, is exclusive for α-Ag$_2$WO$_4$.

4. Conclusions

In summary, we have successfully synthetized MWO$_4$ (M = Cd, Co, Cu, Mn, Ni, and Zn) and α-Ag$_2$WO$_4$ powders that can be used as catalysts in the selective aerobic oxidation of sulfides to sulfones. A variety of sulfides could be directly transformed, showing a broad substrate scope with substantial functional group tolerance. The key success of the selective oxidation is attributed to hydroxyl radical and singlet oxygen (•OH and $^1O_2$), as the redox mediators. Besides, the α-Ag$_2$WO$_4$ catalyst could be facilely recycled at least ten times without losing effectiveness and, with a slight decrease in the catalytic activity in the case of the NiWO$_4$. To the best of our knowledge, this is the first active catalysts for the selective oxidation of sulfides to sulfones in dark. This study takes

advantage of a catalyst in full to unravel a multifaceted challenge, not only providing a concise design principle for oxidation processes, but also offering an unrecognized opportunity in chemo- and selective obtention of functionalized sulfones determined by the kinetics of the intrinsic substrate reactivity. Present findings support the potential of these semiconductors materials for their use in academic research and industry not only in various oxidation processes, but also unlock applications as sensors and biocide materials, capitalizing the metal oxide's biocompatibility.

CRediT authorship contribution statement

M.A.: Data curation, Formal analysis, Investigation, Methodology, Writing – original draft, Writing – review & editing, Visualization, Funding acquisition, Resources. **A.F.G.** and **L.K.R.:** Data curation, Writing – original draft, Writing – review & editing. **M.A.P.** and **M.S.S.:** Data curation, Formal analysis, Investigation, Methodology, Writing – original draft, Writing – review & editing. **O.N.O.Jr, L.H.M., R.L., E.L., E.G.** and **J.A.:** Funding acquisition, Resources, Supervision, Writing – original draft, Writing – review & editing, Visualization.

Declaration of Competing Interest

The authors declare that they have no known competing financial interests or personal relationships that could have appeared to influence the work reported in this paper.

Data Availability

Data will be made available on request.

Acknowledgments

Appendix A. Supporting information

Supplementary data associated with this article can be found in the online version at doi:10.1016/j.apcata.2023.119038.

References

[1] S. Liang, K. Hofman, M. Friedrich, J. Keller, G. Manolikakes, Recent progress and emerging technologies towards a sustainable synthesis of sulfones (n/a), ChemSusChem (2021) (n/a).

[2] S. Matavos-Aramyan, S. Soukhakian, M.H. Jazebizadeh, Selected methods for the synthesis of sulfoxides and sulfones with emphasis on oxidative protocols, Phosphorus Sulfur Silicon Relat. Elem. 195 (2020) 181–193.

[3] E. Skolia, P.L. Gkizis, C.G. Kokotos, Aerobic photocatalysis: oxidation of sulfides to sulfoxides, Chempluschem 87 (2022).

[4] Q.W. Fan, L.W. Zhu, X.H. Li, H.J. Ren, G.R. Wu, H.B. Zhu, W.J. Sun, Catalyst-free visible light-mediated selective oxidation of sulfides into sulfoxides under clean conditions, Green. Chem. 23 (2021) 7945–7949.

[5] E. Voutyritsa, I. Triandafillidi, C.G. Kokotos, Green organocatalytic oxidation of sulfides to sulfoxides and sulfones, Synth. -Stuttg. 49 (2017) 917–924.

[6] E. Skolia, P.L. Gkizis, N.F. Nikitas, C.G. Kokotos, Photochemical aerobic oxidation of sulfides to sulfoxides: the crucial role of wavelength irradiation, Green. Chem. 24 (2022) 4108–4118.

[7] E. Skolia, P.L. Gkizis, C.G. Kokotos, A sustainable photochemical aerobic sulfide oxidation: access to sulforaphane and modafinil, Org. Biomol. Chem. 20 (2022) 5836–5844.

[8] C. Drago, L. Caggiano, R.F.W. Jackson, Vanadium-catalyzed sulfur oxidation/kinetic resolution in the synthesis of enantiomerically pure alkyl aryl sulfoxides, Angew. Chem., Int. Ed. 44 (2005) 7221–7223.

[9] Y.M. Li, S. Rizvi, D.Q. Hu, D.W. Sun, A.H. Gao, Y.B. Zhou, J. Li, X.F. Jiang, Selective late-stage oxygenation of sulfides with ground-state oxygen by uranyl photocatalysis, Angew. Chem., Int. Ed. 58 (2019) 13499–13506.

[10] P. Cruz, M. Fajardo, I. del Hierro, Y. Perez, Selective oxidation of thioanisole by titanium complexes immobilized on mesoporous silica nanoparticles: elucidating the environment of titanium(iv) species, Catal. Sci. Technol. 9 (2019) 620–633.

[11] F.Y. Zhang, J.L. Zhang, B.X. Zhang, L.R. Zheng, X.Y. Cheng, Q. Wan, B.X. Han, J. Zhang, Improved catalytic performance of Co-MOF-74 by nanostructure construction, Green. Chem. 22 (2020) 5995–6000.

[12] L.Q. Wei, B.H. Ye, Cyclometalated Ir-Zr metal-organic frameworks as recyclable visible-light photocatalysts for sulfide oxidation into sulfoxide in water, ACS Appl. Mater. Interfaces 11 (2019) 41448–41457.

[13] L.F. Liu, B.X. Zhang, X.N. Tan, D.X. Tan, X.Y. Cheng, B.X. Han, J.L. Zhang, Improved photocatalytic performance of covalent organic frameworks by nanostructure construction, Chem. Commun. 56 (2020) 4567–4570.

[14] D. Karimian, F. Zangi, Aerobic photoxidation of sulfides using unique hybrid polyoxometalate under visible light, Catal. Commun. 152 (2021).

[15] J. Dong, J.F. Hu, Y.N. Chi, Z.G. Lin, B. Zou, S. Yang, C.L. Hill, C.W. Hu, A. Polyoxoniobate-Polyoxovanadate, Double-anion catalyst for simultaneous oxidative and hydrolytic decontamination of chemical warfare agent simulants, Angew. Chem. Int. Ed. 56 (2017) 4473–4477.

[16] M. Fadhli, I. Khedher, J.M. Fraile, Modified Ta/MCM-41 catalysts for enantioselective oxidation of thioanisole, J. Mol. Catal. A Chem. 410 (2015) 140–148.

[17] J.J. Li, Y.N. Chen, X. Yang, S.Y. Gao, R. Cao, Visible-light-mediated high-efficiency catalytic oxidation of sulfides using wrinkled C3N4 nanosheets, J. Catal. 381 (2020) 579–589.

[18] N. Moussa, J.M. Fraile, A. Ghorbel, J.A. Mayoral, Catalytic oxidation of thioanisole Ph-S-CH3 over VOx/SiO2 and VOx/Al2O3 catalysts prepared by sol-gel method, J. Mol. Catal. A Chem. 255 (2006) 62–68.

[19] B. Yu, C.X. Guo, C.L. Zhong, Z.F. Diao, L.N. He, Metal-free chemoselective oxidation of sulfides by in situ generated Koser's reagent in aqueous media, Tetrahedron Lett. 55 (2014) 1818–1821.

[20] X.Y. Cheng, J.L. Zhang, L.F. Liu, L.R. Zheng, F.Y. Zhang, R. Duan, Y.F. Sha, Z.Z. Su, F. Xie, Air atmospheric photocatalytic oxidation by ultrathin C,N-TiO2 nanosheets, Green. Chem. 23 (2021) 1165–1170.

[21] C.M. Silva, P.L. Silva, J.R. Pliego, Hydroperoxo on the niobium oxyhydroxide surface as the active species in the catalyzed oxidation of organic sulfide by hydrogen peroxide, J. Phys. Chem. C. 124 (2020) 9369–9375.

[22] I. Triandafillidi, D.I. Tzaras, C.G. Kokotos, Green organocatalytic oxidative methods using activated ketones, Chemcatchem 10 (2018) 2521–2535.

[23] P.V. Kamat, Semiconductor surface chemistry as holy grail in photocatalysis and photovoltaics, Acc. Chem. Res. 50 (2017) 527–531.

[24] Y.Q. Qu, X.F. Duan, Progress, challenge and perspective of heterogeneous photocatalysts, Chem. Soc. Rev. 42 (2013) 2568–2580.

[25] N. Serpone, A.V. Emeline, Semiconductor photocatalysis - past, present, and future outlook, J. Phys. Chem. Lett. 3 (2012) 673–677.

[26] M. Waimbo, G. Anduwan, O. Renagi, S. Badhula, K. Michael, J. Park, S. Velusamy, Y.S. Kim, Improved charge separation through H2O2 assisted copper tungstate for enhanced photocatalytic efficiency for the degradation of organic dyes under simulated sun light, J. Photochem. Photobiol. B: Biol. 204 (2020).

[27] X.A. Lopez, A.F. Fuentes, M.M. Zaragoza, J.A.D. Guillen, J.S. Gutierrez, A.L. Ortiz, V. Collins-Martinez, Synthesis, characterization and photocatalytic evaluation of MWO4 (M = Ni, Co, Cu and Mn) tungstates, Int. J. Hydrog. Energy 41 (2016) 23312–23317.

[28] L.H. Li, Y. Li, Y.Z. Li, A.H. Lu, H.R. Ding, P.K. Wong, H.L. Sun, J.X. Shi, Natural wolframite as a novel visible-light photocatalyst towards organics degradation and bacterial inactivation, Catal. Today 358 (2020) 177–183.

[29] M. Kang, X. Wang, J. Zhang, Y. Lu, X. Chen, L. Yang, F. Wang, Boosting the photocatalytic oxidative desulfurization of dibenzothiophene by decoration of MWO4 (M=Cu, Zn, Ni) on WO3, J. Environ. Chem. Eng. 7 (2019), 102809.

[30] N.A. Lima, L.D.S. Alencar, G.C. Mendonça, A. Mesquita, A.V.P. Silva, M. G. Rosmaninho, J.G. Taylor, H.V. Fajardo, L.C. Moraes, M.I.B. Bernardi, Heterogeneous catalysis for thioanisole oxidation using hydrogen peroxide and Copper, Nickel and Zinc tungstates prepared by the polymeric precursor method, Res. Sq. (2020).

[31] P.F.S. Pereira, A.F. Gouveia, M. Assis, R.C. de Oliveira, I.M. Pinatti, M. Penha, R. F. Goncalves, L. Gracia, J. Andres, E. Longo, ZnWO4 nanocrystals: synthesis, morphology, photoluminescence and photocatalytic properties, Phys. Chem. Chem. Phys. 20 (2018) 1923–1937.

[32] N.G. Macedo, A.F. Gouveia, R.A. Roca, M. Assis, L. Gracia, J. Andrés, E.R. Leite, E. Longo, Surfactant-mediated morphology and photocatalytic activity of α-Ag2WO4 material, J. Phys. Chem. C. 122 (2018) 8667–8679.

[33] Y.L. Oliveira, A.F. Gouveia, M.J.S. Costa, F.H.P. Lopes, J.C. Sczancoski, E. Longo, G.E. Luz Jr, R.S. Santos, L.S. Cavalcante, Investigation of electronic structure,

morphological features, optical, colorimetric, and supercapacitor electrode properties of CoWO4 crystals, Mater. Sci. Energy Technol. 5 (2022) 125–144.

[34] A.F. Gouveia, M. Assis, L.S. Cavalcante, L. Gracia, E. Longo, J. Andres, Reading at exposed surfaces: theoretical insights into photocatalytic activity of ZnWO4, Front. Res. Today 1 (2018).

[35] A.E.B. Lima, R.Y.N. Reis, L.S. Ribeiro, L.K. Ribeiro, M. Assis, R.S. Santos, C.H. M. Fernandes, L.S. Cavalcante, E. Longo, J.A.O. Osajima, G.E. Luz, Microwave-assisted hydrothermal synthesis of CuWO4-palygorskite nanocomposite for enhanced visible photocatalytic response, J. Alloy. Compd. 863 (2021).

[36] L.S. Cavalcante, M.A. Almeida, W. Avansi Jr., R.L. Tranquilin, E. Longo, N. C. Batista, V.R. Mastelaro, M.S. Li, Cluster coordination and photoluminescence properties of alpha-Ag2WO4 microcrystals, Inorg. Chem. 51 (2012) 10675–10687.

[37] E. Longo, L.S. Cavalcante, D.P. Volanti, A.F. Gouveia, V.M. Longo, J.A. Varela, M. O. Orlandi, J. Andres, Direct in situ observation of the electron-driven synthesis of Ag filaments on alpha-Ag2WO4 crystals, Sci. Rep. 3 (2013) 1676.

[38] A.F. Gouveia, R.A. Roca, N.G. Macedo, L.S. Cavalcante, E. Longo, M.A. San-Miguel, A. Altomare, G.S. da Silva, J. Andrés, Ag2WO4 as a multifunctional material: fundamentals and progress of an extraordinarily versatile semiconductor, J. Mater. Res. Technol. 21 (2022) 4023–4051.

[39] P. Nithya, C. Roumana, Unexpected high efficient dye sensitized solar cell based NiWO4 decorated bio activated carbon nanosheets hybrid photoanodes by one-pot facile hydrothermal approach, Inorg. Chem. Commun. 118 (2020).

[40] W. Wang, N. Wu, J.M. Zhou, F. Li, Y. Wei, T.H. Li, X.L. Wu, MnWO4 nanoparticles as advanced anodes for lithium-ion batteries: F-doped enhanced lithiation/delithiation reversibility and Li-storage properties, Nanoscale 10 (2018) 6832–6836.

[41] B.G.S. Raj, J. Acharya, M.K. Seo, M.S. Khil, H.Y. Kim, B.S. Kim, One-pot sonochemical synthesis of hierarchical MnWO4 microflowers as effective electrodes in neutral electrolyte for high performance asymmetric supercapacitors, Int. J. Hydrog. Energy 44 (2019) 10838–10851.

[42] W. Yan, X.C. Liu, S. Hou, X. Wang, Study on micro-nanocrystalline structure control and performance of ZnWO4 photocatalysts, Catal. Sci. Technol. 9 (2019) 1141–1153.

[43] B.J. Rani, G. Ravi, S. Ravichandran, V. Ganesh, F. Ameen, A. Al-Sabri, R. Yuvakkumar, Electrochemically active XWO4 (X = Co, Cu, Mn, Zn) nanostructure for water splitting applications, Appl. Nanosci. 8 (2018) 1241–1258.

[44] A.C. Catto, T. Fiorido, E.L.S. Souza, W. Avansi, J. Andres, K. Aguir, E. Longo, L. S. Cavalcante, L.F. da Silva, Improving the ozone gas-sensing properties of CuWO4, Nanopart., J. Alloy. Compd. 748 (2018) 411–417.

[45] L.O. Laier, M. Assis, C.C. Foggi, A.F. Gouveia, C.E. Vergani, L.C.L. Santana, L. S. Cavalcante, J. Andres, E. Longo, Surface-dependent properties of alpha-Ag2WO4: a joint experimental and theoretical investigation, Theor. Chem. Acc. 139 (2020) 108.

[46] A.I. Cervantes-Macias, C.A. Huerta-Aguilar, T. Pandiyan, ZnO-Fe3O4-Au hybrid composites for thioanisole oxidation under visible light: experimental and theoretical studies, J. Clust. Sci. 28 (2017) 1897–1922.

[47] Y.H. Fan, S.G. Li, J.X. Bao, L. Shi, Y.Z. Yang, F. Yu, P. Gao, H. Wang, L.S. Zhong, Y. H. Sun, Hydrofunctionalization of olefins to value-added chemicals via photocatalytic coupling, Green. Chem. 20 (2018) 3450–3456.

[48] M. Assis, C.C. de Foggi, V. Teodoro, J.P.D. da Costa, C.E. Silva, T. Robeldo, P. F. Caperucci, C.E. Vergani, R.C. Borra, I. Sorribes, A.F. Gouveia, M.A. San-Miguel, J. Andres, E. Longo, Surface-dependent photocatalytic and biological activities of Ag2CrO4: integration of experiment and simulation, Appl. Surf. Sci. 545 (2021), 148964.

[49] F. Barati, M. Grossnickle, S.S. Su, R.K. Lake, V. Aji, N.M. Gabor, Hot carrier-enhanced interlayer electron-hole pair multiplication in 2D semiconductor heterostructure photocells, Nat. Nanotechnol. 12 (2017) 1134.

[50] E. Albiter, S. Alfaro, M.A. Valenzuela, Photosensitized oxidation of 9,10-dimethy-lanthracene with singlet oxygen by using a safranin O/silica composite under visible light, Photochem. Photobiol. Sci. 14 (2015) 597–602.

[51] A. Gomes, E. Fernandes, J. Lima, Fluorescence probes used for detection of reactive oxygen species, J. Biochem. Biophys. Methods 65 (2005) 45–80.

[52] Z.G. Chen, K.X. Xia, X.J. She, Z. Mo, S.W. Zhao, J.J. Yi, Y.G. Xu, H.X. Chen, H. Xu, H.M. Li, 1D metallic MoO2-C as co-catalyst on 2D g-C3N4 semiconductor to promote photocatlaytic hydrogen production, Appl. Surf. Sci. 447 (2018) 732–739.

[53] J. Brame, M.C. Long, Q.L. Li, P. Alvarez, Trading oxidation power for efficiency: differential inhibition of photo-generated hydroxyl radicals versus singlet oxygen, Water Res. 60 (2014) 259–266.

[54] A.C.M. Tello, M. Assis, R. Menasce, A.F. Gouveia, V. Teodoro, N. Jacomaci, M. A. Zaghete, J. Andres, G.E. Marques, M.D. Teodoro, A.B.F. da Silva, J. Bettini, E. Longo, Microwave-driven hexagonal-to-monoclinic transition in BiPO4: an in-depth experimental investigation and first-principles study, Inorg. Chem. 59 (2020) 7453–7468.

[55] J.R. Harbour, S.L. Issler, Involvement of the azide radical in the quenching of singlet oxygen by azide anion in water, J. Am. Chem. Soc. 104 (1982) 903–905.

[56] C. Yin, T. Ye, Y.W. Yu, W.M. Li, Q.G. Ren, Detection of hydroxyl radicals in sonoelectrochemical system, Microchem. J. 144 (2019) 369–376.

[57] D.I. Foustoukos, J.L. Houghton, W.E. Seyfried, S.M. Sievert, G.D. Cody, Kinetics of H-2-O-2-H2O redox equilibria and formation of metastable H2O2 under low temperature hydrothermal conditions, Geochim. Cosmochim. Acta 75 (2011) 1594–1607.

[58] L. Yang, B. Kruse, Revised Kubelka-Munk theory. I. Theory and application, J. Opt. Soc. Am. A: Opt. Image Sci. Vis. 21 (2004) 1933–1941.

[59] Y. Nosaka, A.Y. Nosaka, Generation and detection of reactive oxygen species in photocatalysis, Chem. Rev. 117 (2017) 11302–11336.